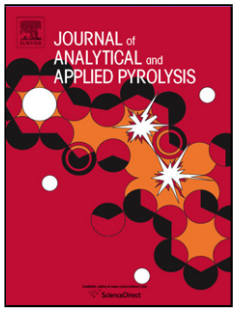

Title: TGA-FTIR study of the thermal and SBA-15-catalytic pyrolysis of potassium citrate under nitrogen and air atmospheres

Author: A. Marcilla A. Gómez M. Beltrán D. Berenguer I. Martínez I. Blasco

PII: S0165-2370(16)30775-6
DOI: http://dx.doi.org/doi:10.1016/j.jaap.2017.04.007
Reference: JAAP 4017

To appear in: *J. Anal. Appl. Pyrolysis*

Received date: 23-11-2016
Accepted date: 11-4-2017

Please cite this article as: A. Marcilla, A. Gómez, M. Beltrán, D. Berenguer, I. Martínez, I. Blasco, TGA-FTIR study of the thermal and SBA-15-catalytic pyrolysis of potassium citrate under nitrogen and air atmospheres, *Journal of Analytical and Applied Pyrolysis* (2017), http://dx.doi.org/10.1016/j.jaap.2017.04.007

TGA-FTIR study of the thermal and SBA-15-catalytic pyrolysis of potassium citrate under nitrogen and air atmospheres

A. Marcilla, A. Gómez, M. Beltrán, D. Berenguer, I. Martínez and I. Blasco

Highlights

- A TFG/FTIR study of potassium citrate with and without SBA-15 has been performed
- A decomposition scheme based on 7 reactions is suggested
- Additional oxidation steps appear in air atmosphere
- The final decomposition step would involve the formation of porous carbons
- SBA-15 reduces the number of degradation steps and the yield of volatile compounds

Abstract

In this work, the thermal and SBA-15 catalytic pyrolysis of potassium citrate has been studied by TGA/FTIR. According to the TGA results, in the absence of a catalyst, a decomposition mechanism based on a sequence of four consecutive reactions is proposed, yielding a solid residue plus potassium carbonate, which at temperatures of 650 ^{o}C evolves towards the formation of microporous activated carbons. The reaction scheme in an air atmosphere is quite similar, with the only exception of additional oxidation steps. As a general rule, the presence of SBA-15 as a catalyst seems to reduce the number of decomposition steps and to inhibit the last stages of the formation of porous carbons. The proposed mechanisms are in good agreement with the FTIR analysis of the evolution of the gases evolved at each temperature, as well as with the endothermic or exothermic character of the heat flow involved. A different way to interpret and compare the FTIR intensity data is proposed, which is complementary to the usual analysis based on the normalization with respect to the total amount of sample and permits us to more clearly interpret the role of the catalyst at each temperature. This type of analysis shows that the catalyst actually decreases the yields of volatile compounds obtained at each temperature, and enhances the true effect of the catalyst on the composition of the gases evolved at each temperature.

Introduction

The catalytic effect of alkali metals on the thermal decomposition of biomass has been studied from years [1]. Potassium is a key plant nutrient that significantly affects the pyrolysis and combustion processes of biomass [2] increasing the rate of decomposition and the yield of gas and char, and decreasing tar products [3]. It has been described elsewhere that potassium promotes the formation of low molecular weight pyrolysis products and suppresses the formation of levoglucosan [4, 5].

Potassium salts are widely used as additives in cigarette manufacturing with different objectives and so, the knowledge of the pyrolytic behaviour of these salts is a subject of interest for the tobacco industry and applied research. The use of potassium citrate as a flavoring agent was reported by Baker et al. [6, 7]. Potassium sorbate is used as a preservative and mold growth inhibitor [6, 8]. The influence of potassium lactate, malate and tartrate on the combustion behavior and mainstream smoke of cigarettes has also been studied [9-13]. The general consequence of the addition of alkali compounds in cellulose or in biomass pyrolysis is a change in the distribution and composition of the pyrolysis products, with the decrease of tar yields and the increase of the formation of char and gaseous products, as well

as the decrease of the temperature of pyrolysis [1-5]. This is the reason why potassium carboxylates are used as combustion improvers in cellulosic cigarette paper [14, 15, 16].

According to the bibliography [17-21], the mechanism of biomass pyrolysis is complicated and involves a large number of parallel and series reactions; nevertheless, a realistic approach can be made considering three independent parallel reactions, each corresponding to the decomposition of the constituent components hemicellulose, cellulose and lignin. Nevertheless, the pyrolytic reactions of potassium citrate have not been extensively studied. The pyrolysis of citric acid and other citrate salts has been described [22-25], in general involving three or four decomposition stages. Moldoveanu [26] has reported the mechanisms and products of the pyrolysis of citric acid, stating that when heated at low temperatures and for a longer time yields aconitic acid; further heating leads to itaconic anhydride, which isomerizes into citraconic anhydride. Barbooti and Al-Sammerrai [22] stated that the thermal decomposition reactions of citric acid were influenced by the particle size of the sample and the heating rate employed. The pyrolysis of carboxylic acid salts is a complex subject because it is affected by many parameters, such as the nature of the acid, the nature of the metal and the pyrolysis conditions [26]. Other studies, focused on the use of a citrate route to obtain laminated activated carbons [27, 28], described the mechanism of the decomposition of potassium citrate as a series of reactions within the 200-500 ^{o}C temperature range, leading to a carbonaceous residue. Further decomposition of this material leads to carbon and potassium carbonate that further decompose into carbon dioxide and potassium oxide (at 700-900 ^{o}C). Carbon dioxide may react with the carbon of the residue and this may react with the potassium oxide to give carbon monoxide and potassium metal that may play a crucial role in the generation of highly porous carbons.

Recently, the use of different porous structured solids has been studied to reduce the evolution of different compounds from tobacco smoke in order to reduce its toxicity [29, 30], and the effect of these materials on the pyrolysis reactions of different tobacco additives has been studied using TG and TG-FTIR techniques [20, 21]. The objective of the present paper is to study the thermal decomposition of potassium citrate by TG-FTIR and the effect of SBA-15 in such reactions both in N_2 and in air atmospheres, which to our knowledge has not been reported previously.

In addition, we propose a new point of view in order to interpret and analyze the TG-FTIR data. In fact, the most frequent approach for carrying out the comparison among the FTIR or heat flow data of different samples consists in the normalization of the absorbance data by dividing by the mass of sample [1, 14]. Nevertheless, the decomposition rate changes through the different steps involved in the decomposition process, and the amount of mass which generates the gases responsible for the successive FTIR spectrum also changes. As an example, imagine the comparison between the normalized data of absorbance (absorbance/mg of total amount of sample) obtained from the TG-FTIR analysis of a sample and from the same sample mixed with a catalyst; in order not to perturb the data, only the mass of pyrolyzable sample is considered for the normalization, i.e., the mass of catalyst is not considered. If, at a certain temperature, both samples show an IR-band with the same intensity, expressed in absorbance units/mg of sample, it may be correctly concluded that the respective yield for the compound responsible for this band is similar at the considered temperature and, perhaps incorrectly, that the catalyst does not affect the process generating that compound. Nevertheless, if we normalize dividing by the weight derivative with respect to time, or by the instantaneous amount of mass decomposed, we obtain a closer approach to the particular signal relative

intensity corresponding to that time, and thus magnify the differences of behavior due to the presence of the catalyst. Effectively, let us consider, for instance, the case where the value of absorbance/mg was the same in both cases, but the decomposition rate at the moment considered was higher in the catalyzed process. The usual analysis of TG-FTIR data will lead us to conclude that both samples behave in a similar way and, consequently, the catalyst has no effect. Nevertheless, the amount of gases reaching the FTIR detector would be different in both cases (higher in the catalyzed case), and the intensity in terms of absorbance/instantaneous mass decomposed will be lower in the presence of a catalyst. This suggests therefore that, at the considered temperature, the catalyst reduces the generation of the compound responsible for the considered FTIR band. Then, in order to obtain complementary information about the catalytic effect of SBA-15 on the thermal decomposition of potassium citrate, a different way for the analysis and interpretation of the TG-FTIR data has been applied in this work, by carrying out the normalization of the absorbance data on the basis of the amount of mass decomposed in each interval of time. To do this, we have extracted the FTIR spectra obtained at different temperatures, and we have divided the absorbances obtained by the amount of mass decomposed in that interval (Δw), i.e., by the value obtained multiplying the value of the DTG at the temperature corresponding to each FTIR spectrum by the time interval considered for calculating the TG derivative.

Materials and methods

Tripotassium citrate monohydrate (CAS number 6100-05-6, purity >97%) provided by Sigma Alfa Aesar (C, according to the nomenclature employed) and mesoporous SBA-15 as a catalyst (S, according to the nomenclature employed) have been used. The SBA-15 used, with a fiber-like morphology, has been synthesised in our laboratory according to the procedure described by Zhang et al. [31]. Table 1 shows the textural properties, obtained from the N_2 adsorption isotherms at 77 K, measured in an automatic Quantachrome AUTOSORB-6. The isotherm curve was recorded and the surface area was obtained according to the BET method, the pore size distributions were obtained applying the BJH model with cylindrical geometry of the pores and using the de Boer equation for determining the adsorbed layer thickness (t) and the external surface area. The acidity of the materials was measured by temperature-programmed desorption (TPD) of ammonia, performed in a Netzsch TG 209 thermobalance. The samples were previously outgassed in an N_2 flow of 45 ml/min by heating at 500°C at a rate of 10°C/min, maintaining this temperature for 30 min. After cooling to 100°C, the acid sites were saturated by treatment with an ammonia flow of 35 ml/min for 30 min. The physisorbed ammonia was removed by using a N_2 flow of 45 ml/min for 60 min at 100°C. Finally, the TPD measurements were carried out by heating the sample in the N_2 flow with a rate of 10°C/min up to 900°C. The acidity of the materials was calculated using the weight loss observed in the thermobalance TPD experiments. As seen in Table 1, the catalyst has a neutral character.

Samples of around 5 mg of potassium citrate and 50% (w/w) mixtures of potassium citrate (C) and SBA-15 were pyrolyzed up to 850 ^{o}C in a Metler Toledo thermobalance at a heating rate of 35 ^{o}C/min under a gas (N_2 or synthetic air) flow of 80 mL min^{-1} (STP), connected to a Bruker Tensor 27 FTIR spectrometer through a heated line (200 ^{o}C). In order to improve the contact degree between the organic salt and the catalyst, a small quantity of mixture was prepared, and the minimum quantity of water needed to solve the citrate was added; then the sample was mixed thoroughly with a needle, heated at 60 ^{o}C for 24 h in an oven, and stored in a 60 % of relative humidity environment in order to ensure that the initial adsorbed moisture of all

the samples was the corresponding to phases equilibrium. For comparison, the samples of pure citrate were treated exactly in the same way as the citrate-SBA-15 mixtures.

In the TGA-FTIR runs, the sample temperature was measured with a thermocouple directly attached to the crucible, i.e., very close to the sample. The heating rate was selected high enough to ensure the quality of the FTIR data obtained [32]. Table 2 shows the nomenclature and composition of the samples.

The results reported correspond to the average of three runs showing average deviations lower than 1% in the mass loss and temperature, lower than 3 % in the heat flow and lower than 5 % in the FTIR intensities.

Results and discussion

TGA results of potassium citrate and potassium citrate-SBA-15 mixtures in N_2 and air atmospheres

Figure 1 shows the weight loss (TGA curves, Figure 1a) as well as the weight loss rate (Figure 1b), obtained as the derivative of the weight loss curves (DTG curves, calculated as the time derivative of the remaining mass percentage) from the TGA analysis, for the different runs performed with pure citrate samples, with and without a catalyst. As can be seen, in the absence of SBA-15 (samples CN and CA), four main processes are observed, as well as others that evolve slowly. Moreover, the influence of the type of atmosphere surrounding the sample does not seem to be especially important at low temperatures. However, above 320 ^{o}C, the processes involved in the decomposition in an air atmosphere take place at lower temperatures than in an N_2 atmosphere. The bibliography describes, for different citrate salts, three or four decomposition stages [22-24], whose assignment is not always carried out. It is interesting to observe that there are no DTG-peaks at temperatures lower than 190 ^{o}C. Thus, it can be concluded that adsorbed moisture, as well as hydration water are lost during the treatment undergone by the samples prior to the TGA-FTIR analysis. According to Figure 1, we suggest the following thermal decomposition steps behavior, which below 320 ^{o}C is similar for both atmospheres, but differs for the two last decomposition stages:

1. Two processes are observed in the range of 190-270 ^{o}C, with peak temperatures of 218 ^{o}C and 254 ^{o}C, respectively. According to Srivastava et al. [24], this could be attributed to the formation of different organic salts through decarboxylation and dehydration of anhydrous citrate. These salts could be those corresponding to the organic acids proposed by Moldoveanu [26] as products from citric acid pyrolysis (potassium aconitates and citraconates), even though, as stated previously, the mechanism of decomposition is very complex and involves many chemical reactions.

2. The main decomposition step takes place in the range of 270-318 ^{o}C, with a peak at 297 ^{o}C. This is a fast process that could correspond to the thermal decomposition of the salts obtained in the previous step.

3. In the 320 ^{o}C - 540 ^{o}C temperature range the behavior changes depending on the type of atmosphere used. In an inert atmosphere (CN sample), there is a wide process, where at least three reactions stages seem to be overlapped, with DTG-peak temperatures at around 333 ^{o}C, 425 ^{o}C, and the main one, at 510 ^{o}C, which may correspond to the decomposition of the different products obtained as a result of the previous pyrolysis step, probably to yield potassium carbonate (main peak) and coke.

On the other hand, the shape of the DTG-peak obtained in an air atmosphere (CA sample) also suggests the existence of overlapped processes that proceed at lower temperature than in the inert atmosphere (DTG-peak temperature of around 420 ^{o}C); this peak has been attributed to the oxidation -combustion- of the materials obtained in the previous step, also yielding potassium carbonate. The expected final product in this range of temperature is potassium carbonate (which melts at 891 ^{o}C and decomposes before boiling); nevertheless, the comparison between the amount of the residue obtained at 590 ^{o}C in each case (around 68.35 % and 69.7% in N_2 and air, respectively) with the stoichiometric ratio between potassium carbonate and the anhydrous citrate (45.1%), it seems that other products besides K_2CO_3 are formed. This allow us to conclude that the difference between the actual solid residue at 590 ^{o}C and the theoretical percentage if all the initial potassium citrate was converted to potassium carbonate (23.3 % and 24.6 % for CN and CA, respectively) is the result of coke formation.

4. A slow process starts at around 650 ^{o}C, showing the highest rate at around 830 ^{o}C, being more marked in the presence of an inert atmosphere. This decomposition step may be related to the thermal decomposition of potassium carbonate, among other residual compounds, to yield highly porous activated carbon, as reported by Sevilla and Fuertes [27, 28]. These authors propose the formation of carbon and potassium carbonate that further decompose into carbon dioxide and potassium oxide. Carbon dioxide may react with the carbon of the residue and this may react with the potassium oxide to give carbon monoxide and potassium metal that may play a crucial role in the generation of highly microporous carbons. No more indication regarding the formation of the carbonaceous residue is provided in these papers [27, 28] since the objective was the study of the activated carbon obtained and, in fact, it should be better considered as coke than as carbon. It is worth to point out that in the supplementary material [28], the TG obtained by theses authors is completely similar to that shown in Figure 1 for the CN sample.

According to the previous description, dry potassium citrate (C), may undergo the following reactions, in an N_2 atmosphere:

At moderate temperatures:

$$C \rightarrow R_1 + V_1 \quad (1)$$

$$R_1 \rightarrow R_2 + V_2 \quad (2)$$

$$R_2 \rightarrow R_3 + V_3 \quad (3)$$

$$R_3 \rightarrow R_4 + V_4 + K_2CO_3 \quad (4)$$

At high temperatures:

$$K_2CO_3 \rightarrow K_2O + CO_2 \quad (5)$$

$$R_4 + CO_2 \rightarrow R_5 + V_5 + CO \quad (6)$$

$$R_6 + K_2O \rightarrow R_7 + 2K + CO \quad (7)$$

where C is the anhydrous citrate, R_1 and R_2 are different mixtures of organics salts, probably including aconitates and citraconates, R_3 is the result of the pyrolysis of R_2, which decomposes in a later step (4) yielding the solid residue R_4 and potassium carbonate. V_i, with I = 1 to 5, (I = 1

to 5) represents the complex mixture of volatile materials evolved in each step. R_5, R_6 and R_7 are the different solids involved in the formation of the activated carbon. In the experimental conditions employed in this work, processes (1) to (4) take place at temperatures lower than 540 ^oC, with maximum reaction rates at around 218 ^oC, 254 ^oC, 297 ^oC and 510 ^oC, respectively. Actually, reaction (4) represents the different processes in the range of 320 ^oC - 540 ^oC. Processes (5) to (7) occur in the range of 650 ^oC - 850 ^oC and reflect the formation of microporous activated carbon. The reaction scheme in an air atmosphere is quite similar to that represented by reactions (1) to (7), with the only exception of an additional oxidation step which may substitute, totally or partially, the pyrolysis step (4):

$$R_3 \rightarrow R_4' + CO + CO_2 + H_2O + K_2CO_3 \qquad (4')$$

Figure 1 also shows the effect of the presence of SBA-15 on the pyrolysis of potassium citrate. As can be seen, in the presence of an N_2 atmosphere, the process seems to be simplified, and fewer decomposition steps are observed. There is a preliminary step, at temperatures lower than 100 ^oC (DTG peak at around 78 ^oC), attributed to the catalyst moisture loss. The TGA curve of pure SBA has been also included in Figure 1a in order to show that, actually, the first weight loss event in the samples including catalyst corresponds to the loss of the equilibrium moisture at 60 % relative humidity atmosphere. Apparently, the main effect of the catalyst results in lowering the number of decomposition steps: in fact, the two processes observed, with maxima at 218 ^oC and 254 ^oC could have disappeared, and the first thermal decomposition step is the one observed at around 290 ^oC, which may correspond to the main pyrolysis step that in the absence of a catalyst appears at temperatures slightly higher (around 297 ^oC). The behavior of the sample in the range of 320 ^oC - 540 ^oC is relatively close to that observed in the absence of a catalyst, and mainly the above-mentioned slight displacement towards lower temperatures is observed. Nevertheless, it seems that the presence of SBA-15 inhibits the latter process related to the formation of the highly porous activated carbon observed at temperatures higher than 650 ^oC. The catalytic decomposition in an air atmosphere is very similar to that observed in an inert atmosphere: the process starts with the loss of the catalyst moisture, the processes associated with the dehydration and decarboxylation of citrate, as well as the last decomposition of citrate to yield porous carbon seems to disappear and the pyrolysis step takes place at a slightly lower temperature. However, an additional step, with very low weight loss, occurs at a low temperature (at around 140 ^oC), and the oxidation step, which in the case of the CA sample seems to evolve through several overlapped processes, also seems to evolve by a different route, perhaps as a consequence of changes in the chemical composition of the solid residue oxidized at this step.

As will be discussed in the following sections, simultaneously to the decomposition processes represented by reaction (3), some oxidative processes could also take place in an air atmosphere and in the presence of a catalyst.

TGA-FTIR results of potassium citrate and potassium citrate-SBA-15 mixtures in N_2 and air atmospheres

Figure 2 shows the 3D-FTIR diagram corresponding to the pyrolysis of potassium citrate in an N_2 atmosphere. In this diagram, the FTIR spectra of the gases evolved at each time (i.e., at each TGA temperature) is shown. Then, not only can the qualitative composition of these gases be obtained at each moment, but also the evolution of this composition with time. The assignment of the IR bands has been performed according to the bibliography [1, 15], and by comparison with the library of the equipment, reflecting the appearance of CO_2 (with the

typical bans at 669, 2320 and 2351 cm^{-1}), CO (bands at 2104 and 2174 cm^{-1}) and water (bands in the range of 3500-2700 cm^{-1} and around 1500 cm^{-1}). The band corresponding to the carbonyl groups (1734 cm^{-1}) together with the bands at around 1209, 1363 and 3014 cm^{-1} can be related to the formation of acetone, by a process similar to that proposed by Moldoveanu [26] for the decomposition of citric acid.

Figure 3 shows one of the most frequent ways to analyze the TGA-FTIR data, based on the study of the evolution with the temperature (or time) of selected IR-bands corresponding to several interesting compounds appearing in the gases evolved. In order to permit the comparison among the different samples, the values of absorbance, extracted from the corresponding 3D diagrams, are divided by the amount of potassium citrate used in each experiment. In Figure 3, the scale of temperature has been corrected in order to avoid the delay of time associated with the displacement of the gases from the TGA furnace to the FTIR cell. The profiles obtained are in good agreement with the suggested assignment of the DTG-peaks and, according to the observed behavior; the following considerations can be performed:

- According to Figure 3a, in the non-catalyzed processes (samples CN and CA), water seems to appear mainly associated with the steps related to the dehydration and decarboxylation of citrate to yield other organic salts (peaks at around 215 and 283 ^{o}C) and, in an air atmosphere (CA sample), with the oxidation step (peak at around 415 ^{o}C). In the presence of a catalyst (CSN and CSA samples), the main evolution of water seems to take place at temperatures lower than 100 ^{o}C, related to the catalyst moisture loss, and is noticeably decreased in the subsequent decomposition steps. At temperatures higher than 270 ^{o}C several maxima of water are observed, corresponding to the decomposition of the different salts formed in the previous stages.
- CO_2 starts to evolve at temperatures higher than 210 ^{o}C (Figure 3b), with a clear maximum in the range of 283-295 ^{o}C, depending on the sample, associated with the main pyrolysis step. Moreover, other secondary peaks appear at higher temperatures in an inert atmosphere (around 329 and 500 ^{o}C for the CN sample and 414 and 487 ^{o}C for the CSN sample), which are more marked in the absence of a catalyst, also related to the subsequent pyrolysis steps. Also, the above-described oxidation processes in the presence of an air atmosphere are clearly related to the CO_2 peaks observed at around 414 ^{o}C in the case of the CA sample and 439 ^{o}C for the CSA sample. The increase of the amount of CO_2 at temperatures higher than 650 ^{o}C is in good agreement with the suggested processes of decomposition of potassium carbonate and other compounds to yield porous activated carbons, processes which are inhibited in the presence of a catalyst. According to reactions (5) to (7), these processes yield CO and CO_2; as can be seen from Figures 3b and 3c, the higher yield of CO_2 obtained from the CA sample in comparison with the CN sample may be related to the subsequent oxidation of the CO evolved in the presence of O_2.
- The CO profiles are shown in Figure 3c. As can be seen and as expected, the more marked CO evolution is obtained in an inert atmosphere, in the range of 440-520 ^{o}C, related to suggested pyrolysis steps yielding potassium carbonate. It is interesting to observe the noticeable increase of CO evolved from the CN sample at higher temperatures, which agrees with the proposed decomposition of carbonates towards activated carbons; nevertheless, as previously commented, in the presence of an air atmosphere, the CO evolved from reactions (6) and (7) is oxidized to CO_2 and, therefore, the CO profile from the CA sample does not show any peak above 650 ^{o}C.
- Figure 3d shows the profiles obtained for the IR band at 1734 cm^{-1}, which has assigned to acetone, based on the citric acid decomposition pathway described by Moldoveanu [26].

Nevertheless, other carbonylic compounds could also be contributing to this band. According to Figure 3d, in the absence of a catalyst (samples CN and CA), two maxima of this absorption band are observed. The first at around 220 ^{o}C (for both samples) and the second at around 423 ^{o}C (CA sample) and 490 ^{o}C (CN sample), which may be related to the decomposition steps involved in reactions (1) to (4) (mainly reactions (1) and (4), according to the respective temperatures). The acetone evolution from the catalyzed cases is quite different depending on the type of atmosphere, and in both cases may be attributed to pyrolytic processes. However, in an N_2 atmosphere, the main maximum appears at around 490 ^{o}C, in the same range as in the absence of a catalyst. In an air atmosphere, it appears at around 283 ^{o}C. In good agreement with the decomposition scheme suggested, at temperatures higher than 650 ^{o}C, there is no evolution of carbonylic compounds. More information about the effect of the catalyst is provided later, in the section devoted to the interpretation of the data on the basis of the instantaneous amount of sample decomposed.

Qualitative study of the thermal character of the different decomposition steps

The thermal character of the different processes observed in the DTG curves can be studied through the DSC [14, 16] or DTA [2] data. In the present work, we have analyzed the heat flow derivative divided by the weight loss derivative as well as the time derivative of the actual temperature of the sample, calculated as the increment of the actual sample temperature divided by the time increment at each temperature. The analysis based on the evolution of the heat flow provides the same information, but the curves obtained seem to show more noise. Then, for complex reactions, the heat flow as provided by the TG equipment may not be adequately interpreted and the two previous functions may help in the analysis. In this case, we have selected for discussion the second of the functions. The values of this function for the four cases under study (thermal degradation of CN, CA, CSN and CSA) are shown in Figure 4. As can be seen, the curves present a typical wavy behavior for all experiments. The nominal value is the heating rate (NHR) of the experiment (i.e.: 35 ^{o}C/min) and the actual heating rate (AHR) oscillates around that value. This wavy behavior begins with an AHR value somewhat lower than the nominal one, higher in the range of 150-550 ^{o}C, and finally lower than the NHR. This global behavior has also been observed in blank experiments, where samples not showing thermal events were checked and thus, we conclude that it is not associated with any thermal event in the sample and is characteristic of the experimental conditions and equipment employed. Nevertheless, there are several features observable overlapping on that wide wave that are associated with the thermal processes experienced by the sample.

In order to analyze the thermal processes revealed by Figure 4, the curves of AHR corresponding to the CN, CA and CSA samples have been represented in Figure 5, together with their corresponding FTIR bands profiles. In this Figure, the values of absorbance of each band have been normalized to the maximum value of 1. Sample CSN has not been included in this analysis because the deviation of its AHR from the wavy behavior is very low and, therefore, its interpretation is more difficult. As can be seen in Figure 5a, there are three endothermic processes coincident with the evolution of acetone and water (218 ^{o}C), water and CO_2 (298 ^{o}C) and water, acetone and CO2 (447-507 ^{o}C) from the CN sample, which may be clearly associated with the decomposition events described by reactions (1), (3) and (4). According to Figure 5b, the same endothermic peaks at relatively low temperatures (204 and 283 ^{o}C) are obtained in the case of the CA sample; nevertheless, in this case, an exothermic peak appears at around 405 ^{o}C which can clearly attributed to the oxidation (combustion processes). This exothermic peak may shield a simultaneous endothermic pyrolysis process

responsible for the acetone evolution. The CO profile has not been represented in Figure 5b because, as Figure 3c reflects, it is not significant for this sample.

The case of the CSN sample is somewhat more difficult to interpret because, as Figure 5c indicates, only one exothermic peak at around 283 ^{o}C is observed. Nevertheless, the evidence obtained in this range of temperature (the behavior of the other samples as well as the formation of carbonylic compounds from the CSN sample) suggests the existence of some type of endothermic pyrolytic processes. Thus, in this case, it seems that exothermic oxidative processes may overlap. The combustion processes in the range of 400-450 ^{o}C could also be reflected in the shape of the AHR curve.

Study of the FTIR spectra obtained at each temperature normalized on the basis of the instantaneous amount of sample decomposed.

The qualitative study carried out in a previous section was based on a normalization of the absorbance data with respect to the initial mass of citrate. In this way, we can compare the yields of the different compounds obtained from each sample. As an example, looking at Figure 3d, we can conclude that the yield of acetone (or other carbonylic compounds) obtained from potassium citrate in an inert atmosphere at around 498 ^{o}C is higher in the absence than in the presence of SBA-15. This analysis is correct but does not permit more precise information to be obtained about the effect of the catalyst, as we pointed out in the introduction section because it does not take into account the amount of sample decomposed in the narrow interval of time where the temperature is around 498 ^{o}C. The key is that in the previous analysis the yields were referred to the initial amount of citrate. In this work, we suggest that very interesting and useful information can be obtained from the following study, carried out on the basis of the instantaneous amount of sample decomposed. To do this, we have extracted the FTIR spectra obtained at different temperatures, and we have divided the obtained absorbances by the amount of mass decomposed in that interval ($\Delta w(T) = DTG(T)\cdot\Delta t$).

Figure 6 shows the comparison between the normalized selected spectra corresponding to the gases evolved from the four cases studied in this work. For each case, the extraction of spectra started from the temperature at which, according to Figure 1, the weight loss begins (at around 180 ^{o}C for the non-catalyzed CN and CA samples, and 50 ^{o}C for the catalyzed ones, CSN and CSA), after checking in the corresponding 3D diagrams that there was no significant FTIR signal below such temperatures. Moreover, the extraction of spectra corresponding to the catalyzed systems (CSN and CSA) was finished at around 550 ^{o}C, because no weight loss was observed above this temperature. In order to make the comparison easier, the same scale of absorbance has been maintained in the four cases. The first noticeable observation when we compare the non-catalyzed and the catalyzed samples in each atmosphere (CN - CSN and CA - CSA) is, in general, the lower intensity of the FTIR-peaks obtained in the presence of the catalyst. This reflects that the ability of SBA-15 for reducing the evolution of the volatile compounds is not a consequence of the decomposition of a lower amount of citrate or of the different decomposition rate but actually indicates that the catalyst causes a decrease of the yields of volatile compounds obtained at each temperature. On the other hand, the comparison between the runs performed in inert and in air atmospheres (CN-CA and CSN-CSA) reflects that the evolution of other compounds different than CO_2 and water has been practically eliminated in the oxidizing atmosphere.

The noticeable interest of this type of data analysis can be clearly seen in Figure 7, where the evolution of the absorbance of selected FTIR bands, referred to the weight derivative at each instant is shown. In order to facilitate the comparison, only the range of temperature of 200-550 ^{o}C is shown, which is the one common for the four samples, as seen in Figure 6 (red rectangles highlight this range in Figure 6). The profiles obtained are quite different to those presented in Figure 3, where the normalization of absorbance was carried out by taking into account the total amount of citrate used in each experiment. The first observation is that, as opposed to Figure 3, the behavior observed in Figure 7 does not follow a tendency which could clearly relate with the weight loss episodes reflected by the DTG curves (Figure 1). This indicates therefore, that the previous interpretation of the evolution of the gases is completely influenced by the total amount of sample decomposed in each degradation step. Therefore, a more realistic idea of the influence of the type of atmosphere used or the effect of the addition of a catalyst can be obtained by the comparison of the absorbances referred to the instantaneous amount of mass decomposed. As an example, the profiles obtained in terms of absorbance/mg decomposed suggest that, in the most part of the range of temperatures considered, the evolution of CO_2 (Figure 7a) from samples CN and CSN is relatively similar, but in the range of 250-310 ^{o}C, corresponding to the thermal decomposition of salts, the catalyst reduces drastically the formation of CO_2. Nevertheless, the comparison of the profiles shown in Figure 3b indicated very similar yields in both cases. Both conclusions are correct, but the noticeable differences observed in Figure 7a are related to the reduction of the thermal degradation processes taking place in this interval, whereas the similarities observed in Figure 3b are related with the lower amount of citrate decomposed (the CSN sample contained 50% of catalyst and yields 68% of solid residue at 850 ^{o}C. The residue obtained from pure citrate was however 47%; thus around 32% of the initial citrate in CSN is converted to volatile products, compared to 57% of conversion corresponding to the CN sample). As expected, the yield of CO_2 increases in samples decomposed in an air atmosphere (CA and CSA) in the ranges of temperature where the combustion and oxidation processes occur, and Figure 7a also reflects the effect of the catalyst reducing these processes. Similar conclusions can be obtained from Figures 7b and 7c, where the ability of the catalyst to decrease the yields of CO and acetone and other carbonylic compounds at temperatures lower than 470 ^{o}C, both in N_2 and air atmospheres, is clearly manifested. In fact, according to Figure 3c, the maximum yield of CO is obtained from CN sample, followed by CSN and CSA, and being almost negligible for CSA, and taking place the main CO event generation at around 500 ^{o}C, i.e., the temperature at which the main pyrolysis and/or oxidation processes take place. Nevertheless, according to Figure 7c, in this range of temperature, the behavior of the pyrolysis and oxidation reactions seems to be relatively similar for all the samples; however, clear events of CO generation from CA sample appear at around 268 ^{o}C and 341 ^{o}C, clearly related with the decarboxylation and thermal degradation steps. These events also could occur in less extension in the case of CN sample, but seem to be removed in the presence of catalyst (CSN and CSA samples). The same comments can be applied to the acetone and other carbonylic compounds, when we compare Figures 3b and 7c, thus agreeing to the assignment of the decomposition steps and enhancing the interest of this kind of analysis, based on the instantaneous amount of sample decomposed.

Conclusions

The results obtained suggest that the thermal decomposition of potassium citrate proceeds in a similar way in N_2 and air atmospheres below 320 ^oC, but differs in the last decomposition stages. Between 190-270 ^oC, two processes are observed, attributed to the formation of different organic salts through decarboxylation and dehydration of anhydrous citrate. The main decomposition step is a fast step in the range of 270-318 ^oC, where the thermal decomposition of the salts obtained in the previous step occurs. The behavior in the range of 320 ^oC - 540 ^oC depends on the type of atmosphere used, and in an inert atmosphere may correspond to the decomposition of the different products obtained in the previous pyrolysis step, probably to yield potassium carbonate, whereas in an air atmosphere the combustion of such as materials overlaps. Another process starting at around 650 ^oC is observed, attributed to the thermal decomposition of potassium citrate, among other residual compounds, to yield highly porous activated carbon. This last step is more marked in the presence of an inert atmosphere. The addition of SBA-15 as a catalyst seems to reduce the number of decomposition steps and completely inhibits the last process related to the formation of porous activated carbon. The profiles observed for several chemical species (H_2O, CO_2, CO and acetone as representative of carbonylic compounds) in the gases evolved at each temperature are in good agreement with the proposed decomposition schemes. The thermal character of the different processes has been analyzed through the time derivative of the actual temperature of the sample, and the exothermic or endothermic character of the main degradation step also agrees with the suggested mechanism.

A different way to interpret and compare the FTIR intensity data has been performed, based on the study of the FTIR spectra bands normalized on the basis of the instantaneous amount of mass decomposed at each instant (i.e., at each temperature). This type of analysis is complementary to the usual analysis based on the normalization with respect to the total amount of sample, and permits us to more clearly interpret the role of the catalyst at each temperature, and reflects that, actually, the employed catalyst decreases the yield of the volatile compounds obtained at each temperature.

Acknowledgements

Financial support for this investigation has been provided by the Spanish Ministerio de Economía, Industria y Competitividad (CTQ2015-70726-P) and the Generalitat Valenciana (PROMETEO2016-056).

References

[1] D.J. Nowakowski, J.M. Jones, R.M.D. Brydson, A.B. Ross, Potassium catalysis in the pyrolysis behaviour of short rotation willow coppice, Fuel 86 (2007) 2389-2402.

[2] D.J. Nowakowski, J.M. Jones, Uncatalysed and potassium-catalysed pyrolysis of the cell-wall constituents of biomass and their model compounds, J. Anal. Appl. Pyrol. 83 (2008) 12-25.

[3] A. Saddawi, J.M. Jones, A. Williams, Influence of the Alkali metals on the kinetics of the thermal decomposition of biomass, Fuel Process. Technol. 104 (2012) 189-197.

[4] I.-Y. Eom, J.-Y. Kim, T.-S. Kim, S.-M Lee, D. Choi, I.-G Choi, J.-W Choi, Effect of essential inorganic metals on primary thermal degradation of lignicellulosic biomass, Bioresource Technol. 104 (2012) 687-694.

[5] M. Noshimura, S. Iwasaki, M. Horio, The role of potassium carbonate on cellulose pyrolysis, J. Taiwan Inst. Chem. E. 49 (2009) 630-637.

[6] R.R. Baker, E.D. Masses, G. Smith, An overview of the effects of tobacco ingredients on smoke chemistry and toxicity, Food. Chem. Toxicol. 42S (2004) S53-S83.

[7] R.R. Baker, J.R. Pereira da Silva, G. Smith, The effect of tobacco ingredients on smoke chemistry- Part I: Flavourings and additives, Food. Chem. Toxicol. 42S (2004) S3-37.

[8] C.L. Gaworski, R. Lemus-Olalde, E.L. Carmines, Food. Chem. Toxicol. 46 (2008) 339-351.

[9] C. Yin, Z. Xu, J. Shu, H. Wang, Y. Li, W. Sun, Z. Zhou, M. Chen, F. Zhong, Study on the effect of potassium lactate additive on the combustion behavior and mainstream smoke of cigarettes, J. Therm. Anal. Calorim. 115 (2014) 1733-1751.

[10] K. Izawa, M. Matsukura, Y. Ishizu, Curie-point pyrolysis of cellulose in the presence of potassium malate, Agric. Biol. Chem. 54 (1990) 957-963.

[11]. T. Yamamoto, S. Umemura, H. Kaneko, Effect of exogenous potassium on the reduction in tar, nicotine and carbon monoxide deliveries in the mainstream smoke of cigarettes, Beitr. Tabakforsch. 14 (1990) 379-385.

[12] C. Liu and A. Parry, Potassium organic salts as burn additives in cigarettes, Beitr. Tabakforsch. 20 (2003) 341-347.

[13] W. Gao, K. Chen, R. Yang, F. Yang, Process for coating of reconstituted tobacco sheet with citrates, J. Anal. Appl. Pyrol. 114 (2015) 138-142.

[14] D. Zhao, K. Chen, F. Yang, G. Feng, Y. Sun, Y. Dai, Thermal degradation kinetics and heat properties of cellulosic cigarette paper: influence of potassium carboxylate as combustion improver, Cellulose 20 (2013) 3205-3217.

[15] D. Zhao, Y. Dai, K. Chen, Y. Sun, F. Yang, K. Chen, Effect of potassium inorganic and organic salts on the pyrolysis kinetics of cigarette paper, Anal. Appl. Pyrol 102 (2013) 114-123.

[16] H. Li, Y. Liu, D. Li, B. Cai, Y. Chen, Z. Cheng, Effect of combustion improver on combustion behavior of cigarette paper by simultaneous TG/DSC detection, Chin. J. Chem. 28 (2010) 1322-1326.

[17] D. vamuka, E. Kakaras, E. Kastanaki, P. Grammelis, Pyrolysis characteristics and kinetics of biomass residuals mixtures with lignite, Fuel 82 (2003) 1949-1960.

[18] A. Gómez-Siurana, A. Marcilla, M. Beltrán, I. Martínez, D. Berenguer, R. García-Martínez, T. Hernández-Selva, Study of the oxidative pyrolysis of tobacco-sorbitol-saccharose mixtures in the presence of MCM-41, Thermochimica Acta 530 (2012) 87-94.

[19] A. Gómez-Siurana, A. Marcilla, M. Beltrán, D. Berenguer, I. Martínez-Castellanos, S. Menargues, TGA/FTIR study of tobacco and glycerol-tobacco mixtures, Thermochimica Acta 573 (2013) 146-157.

[20] A. Gómez-Siurana, A. Marcilla, M. Beltrán, D. Berenguer, I. Martínez-Castellanos, L. Catalá, S. Menargues, TGA/FTIR study of the MCM-41-catalytic pyrolysis of tobacco and tobacco-glycerol mixtures, Thermochimica Acta 587 (2014) 24-32.

[21] A. Marcilla, M.I. Beltrán, A. Gómez-Siurana, D. Berenguer, I. Martínez-Castellanos, Nicotine/mesoporous solids interactions at increasing temperatures under inert and air environments, J. Anal. Appl. Pyrol. 119 (2016) 162-172.

[22] M.M. Barbooti, D. Al-Sammerrai, Thermal decomposition of citric acid, Thermochim. Acta 98 (1986) 119-126.

[23] P. S. Devi, M.S. Rao, Study of the thermal decomposition of lanthanum and chromium citrate hydrates, J. Anal. Appl. Pyrol. 22 (1992) 187-195.

[24] A. Srivastava, P. Singh, V.G. Gunjikar, C.I. Jose, Thermal decomposition of barium citrate, Thermochim. Acta 76 (1984) 249-254.

[25] X.-F., Zhu, J.-K. Yang, Y.-C. Hu, L. Li, X. Wang, W. Zhang, X.-J Sun, Y.-F. Guo, S.-T. Chen, Study on behavior of thermal decomposition of lead citrate $Pb(C_6H_6O_7)\cdot H_2O$, Transactions of Materials and Heat Treatment 35 (2014) 10-14.

[26] S.C. Moldoveanu, Pyrolysis of Organic Molecules with Applications to Health and Environmental Issues, Elsevier, Amsterdam, 2010.

[27] M. Sevilla, S.B. Fuertes, A general and facile synthesis strategy towards highly porous carbons: carbonization of organic salts, J. Mater Chem A (1) (2013) 13738-13741.

[28] M. Sevilla, S.B. Fuertes, Direct synthesis of highly porous interconnected carbon nanosheets and their application as high performance supercapacitors, ACSNAno 8 (2014) 5069-5078.

[29] A. Marcilla, A. Gómez-Siurana, D. Berenguer, I. Martínez- Castellanos, M.I. Beltrán, Reduction of tobacco smoke components yield in commercial cigarette brands by addition of HUSY, NaY and Al-MCM-41 to the cigarette rod, Toxicol. Reports 2 (2015) 152-164.

[30] A. Marcilla, M.I. Beltrán A. Gómez-Siurana, I. Martínez, D. Berenguer, Effect of the concentration of siliceous materials added to tobacco cigarettes on the composition of the smoke generated during smoking, Ind. Eng. Chem. Res. 54 (2015) 1916-1929.

[31] F. Zhang, Y. Yan, H. Yang, Y. Meng, C. Yu, B. Tu, D. Zhao, Understanding Effect of Wall Structure on the Hydrothermal Stability of Mesostructured Silica SBA-15, J. Phys. Chem. B 109 (2005) 8723-8732.

[32] V. Berbenni, A. Marini, G. Bruni and T. Zerlia, TG/FT-IR: an analysis of the conditions affecting the combined TG/spectral response, Thermochim. Acta 258 (1995) pp. 125-133.

Figure captions

Figure 1. a) TGA and b) DTG curves corresponding to the pyrolysis of potassium citrate in the absence and in the presence of catalyst, and in inert and in air atmospheres. TGA curve of pure SBA has been included in order to show the initial moisture loss.

Figure 2. 3D-FTIR diagram corresponding to the pyrolysis of potassium citrate in N_2 atmosphere

Figure 3. Evolution with the temperature of the normalized absorbance of several selected FTIR-bands. a) Water, b) CO_2, c) CO, d) Acetone. The normalization has been performed based on the total amount of citrate in the sample

Figure 4. Nominal (NHR) and actual (AHR) heating rates calculated for pyrolysis of the CN, CA, CSN and CSA samples

Figure 5. Nominal (NHR) and actual (AHR) heating rates and selected FTIR-bands profiles as a function of the temperature for a) CN sample, b)CA sample and c) CSA sample

Figure 6. Normalized spectra of the gases evolved at each temperature from a) CN, b)CSN, c) CA and d) CSA samples. Normalization has been carried out based on the amount of sample decomposed in a small interval around the corresponding temperature. The squares indicate the range of temperature analyzed in Figure 7

Figure 7. Evolution with the temperature of the absorbance of several selected FTIR-bands referred to the instantaneous amount of mass decomposed. a) CO_2, b) CO, c) Acetone

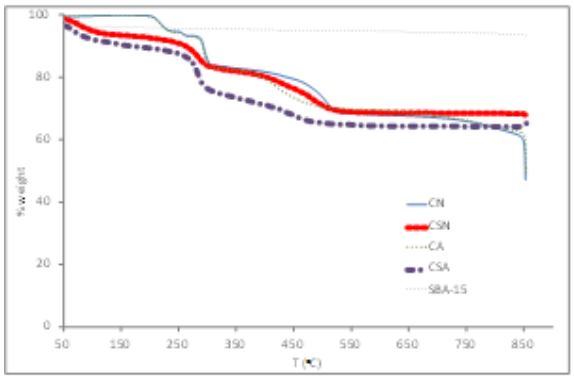

Figr-1

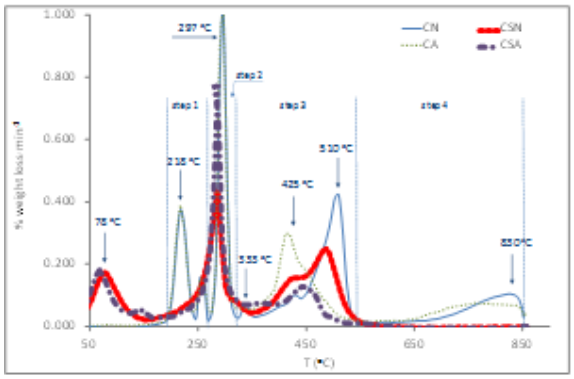

Figr-2

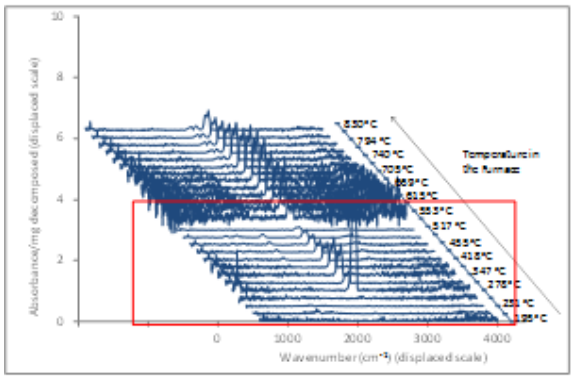

Figr-3

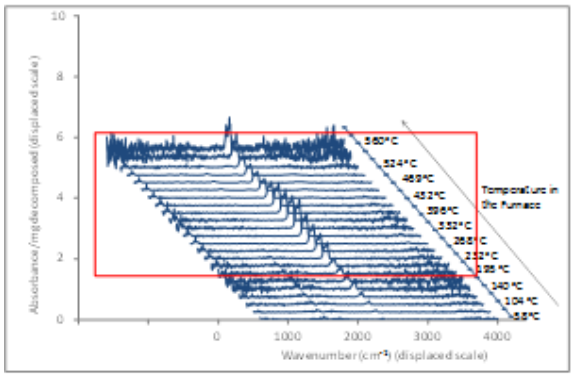

Figr-4

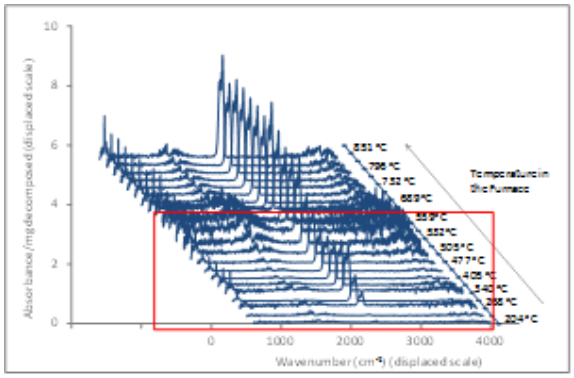

Figr-5

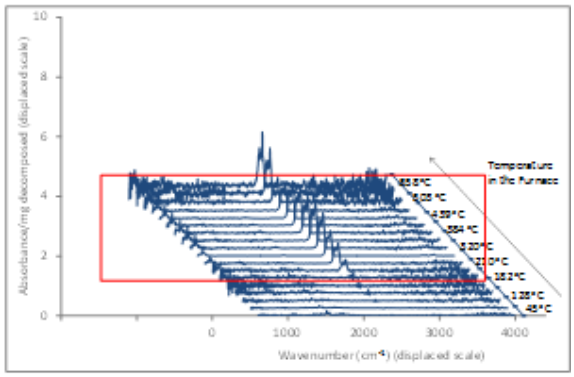

Figr-6

Figr-7

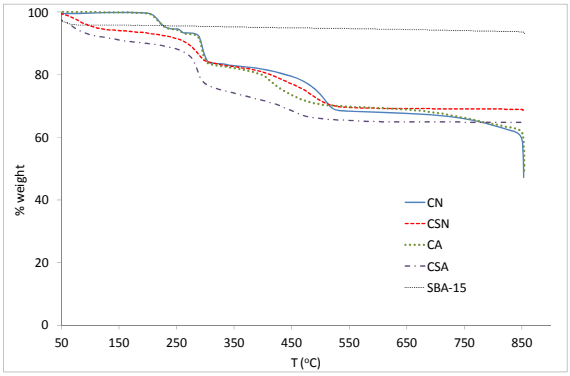

(a)

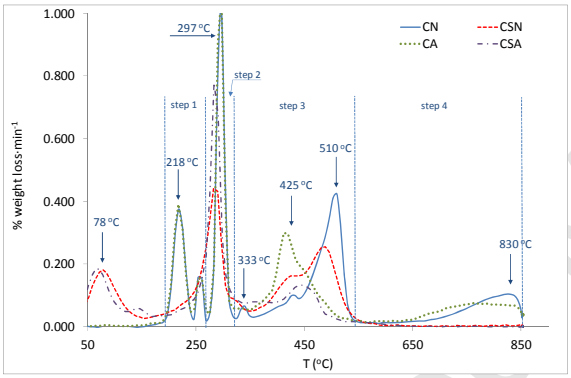

(b)

Figure 1

Figr-

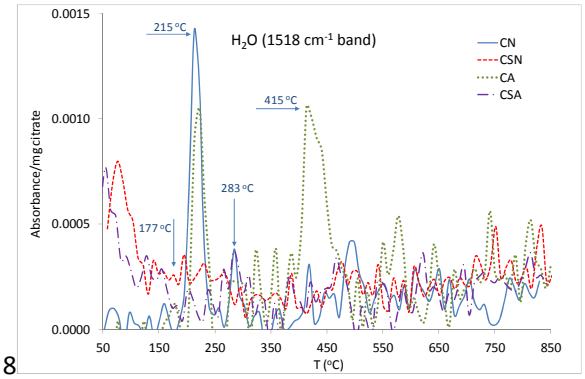

8

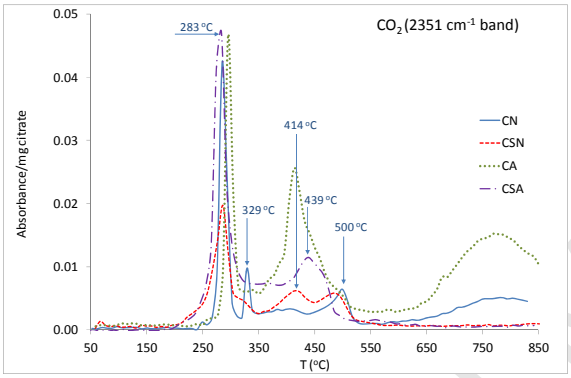

(a)

(b)

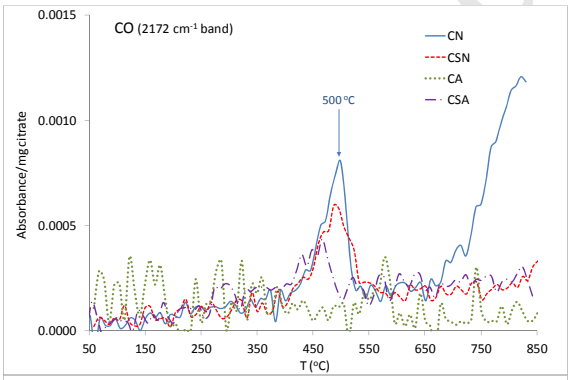

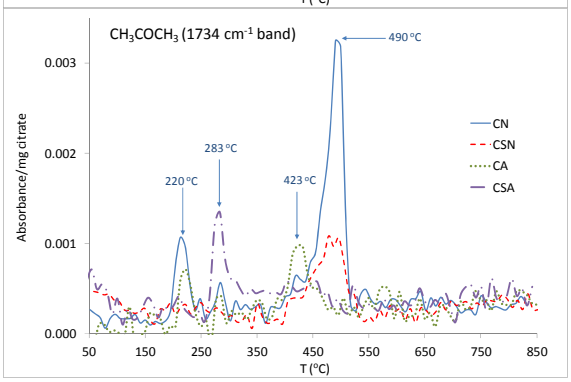

(c)

(d)

Figure 3

Table 1. Characteristics of the catalyst

Catalyst	BET area[1] (m^2/g)	Pores volume[2] (cm^3/g)	Pore size[3] (nm)	Acidity[4] (mmol/g)
S (SBA-15)	757	1.06	6.1	0

1. N_2 adsorption isotherms, BET method
2. N_2 adsorption isotherms, measured at $P/P_0 = 0.995$
3. N_2 adsorption isotherms, BJH method
4. TPD of NH_3

Table 2. nomenclature and composition of samples.

Sample	% potassium citrate	% SBA-15	Atmosphere
CN	100	0	N_2
CSN	50	50	N_2
CA	100	0	Air
CSA	50	50	Air

Figr-9

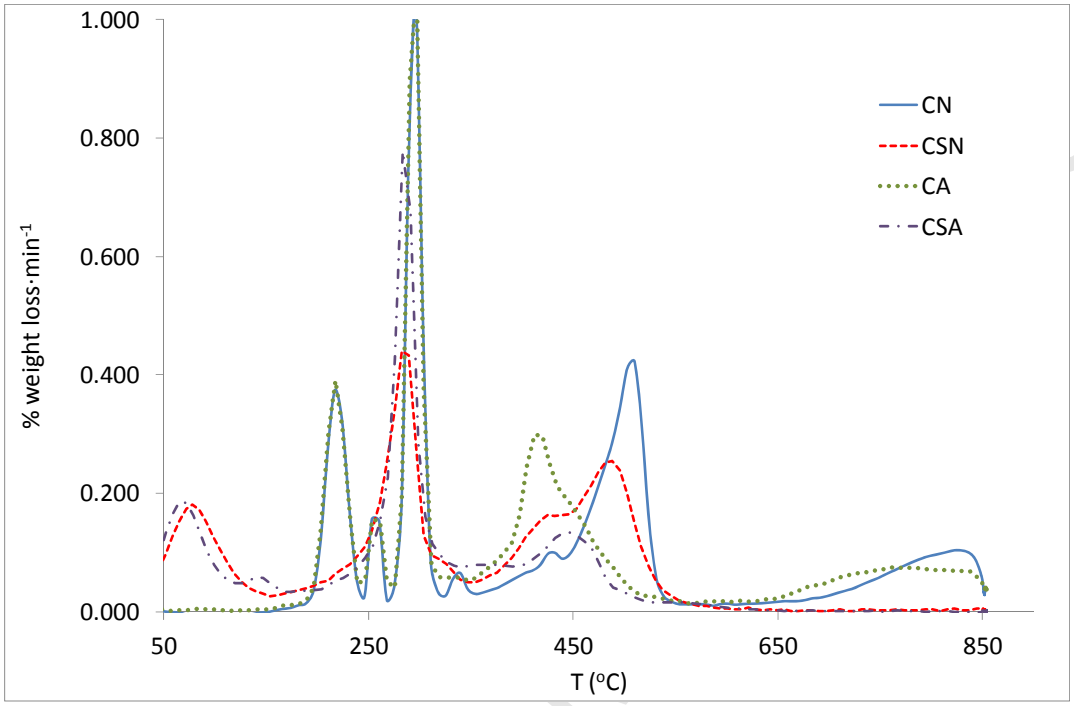

Figure 1.

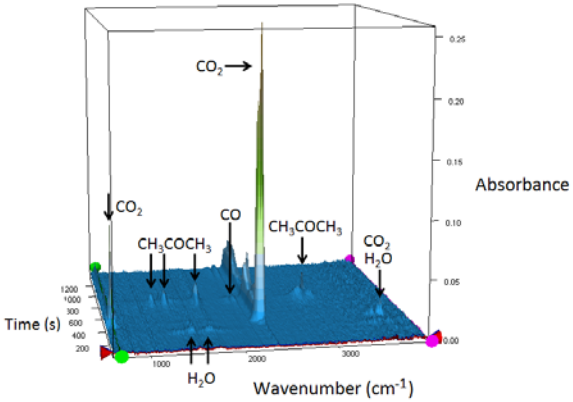

Figure 2.

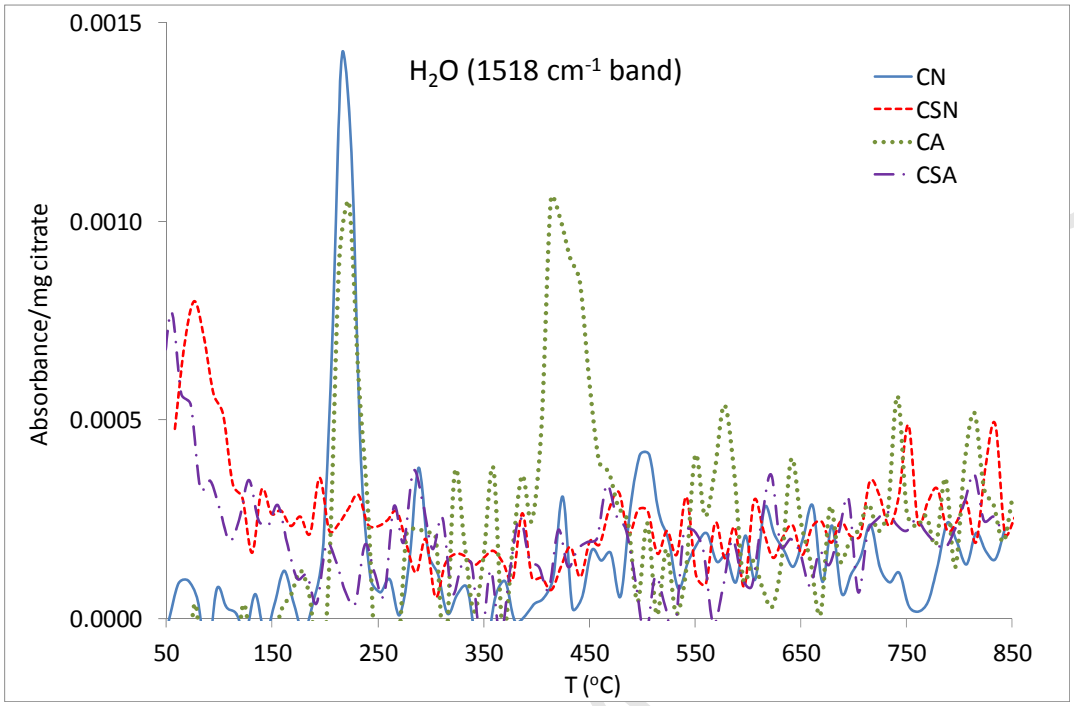

Figure 3a.

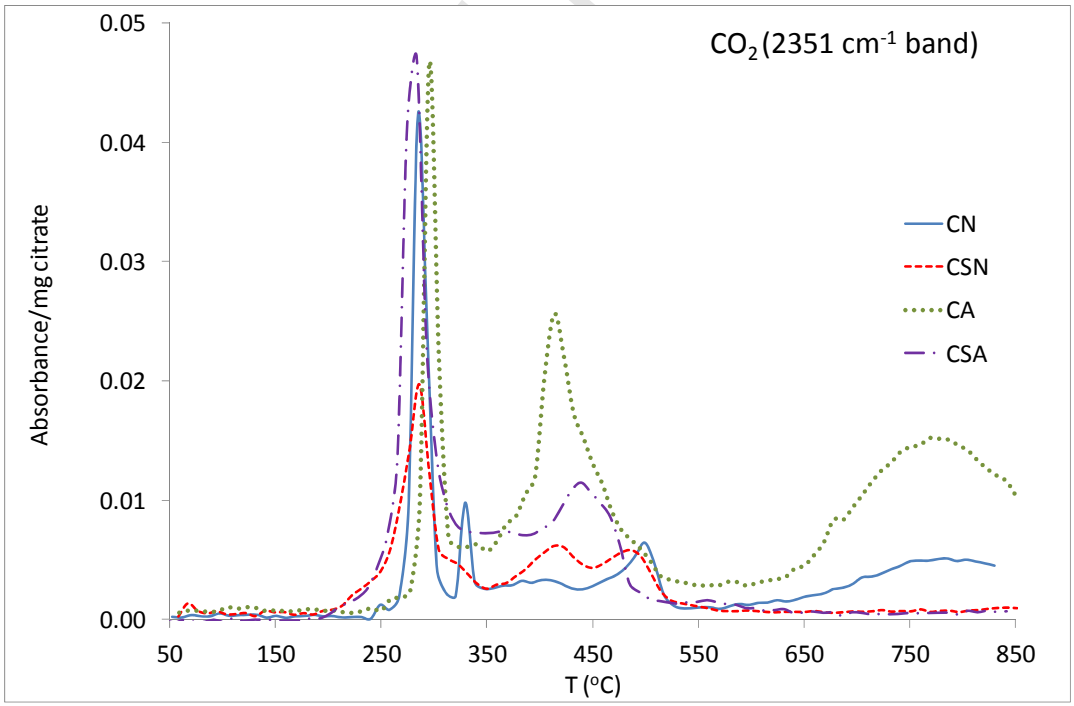

Figure 3b.

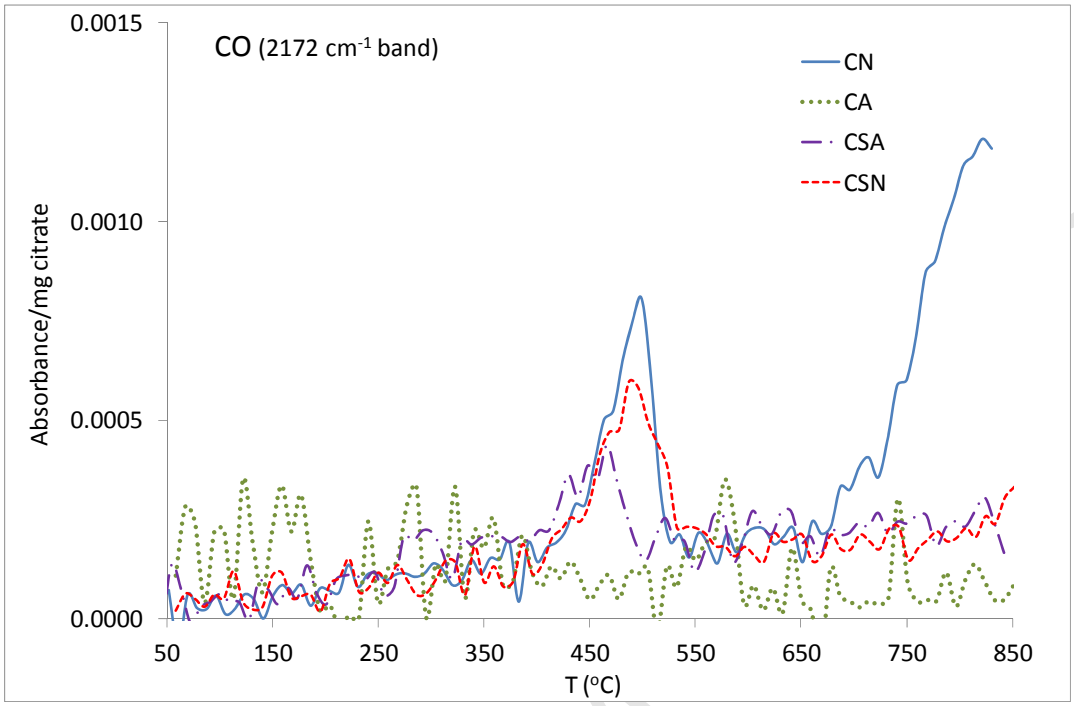

Figure 3c.

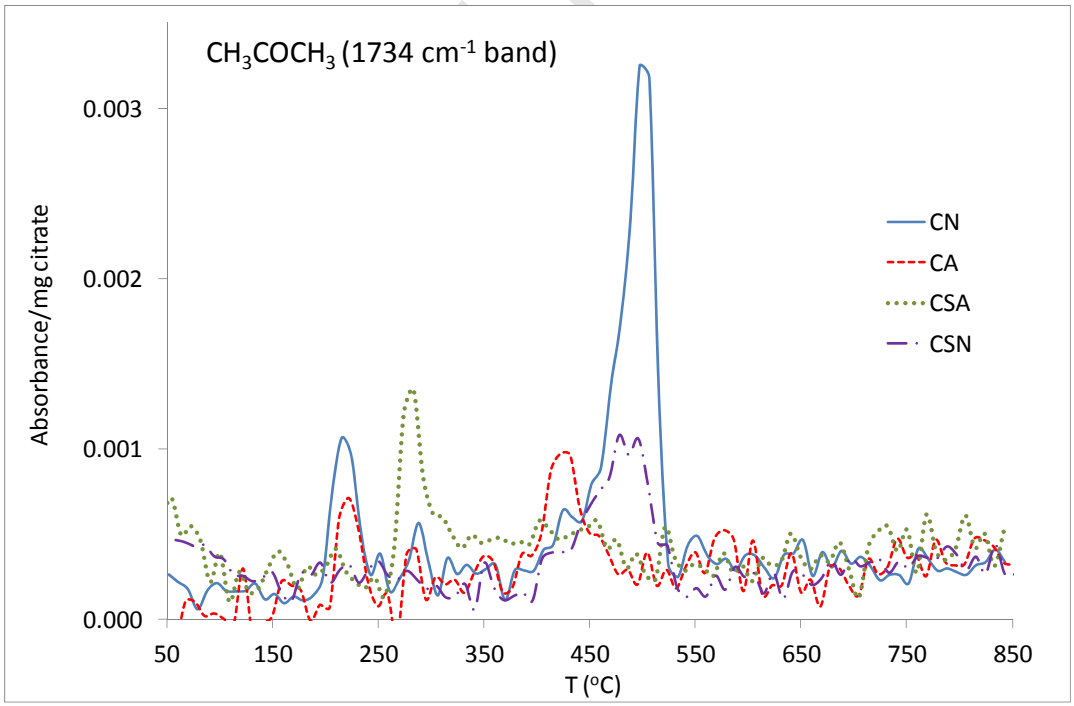

Figure 3d.

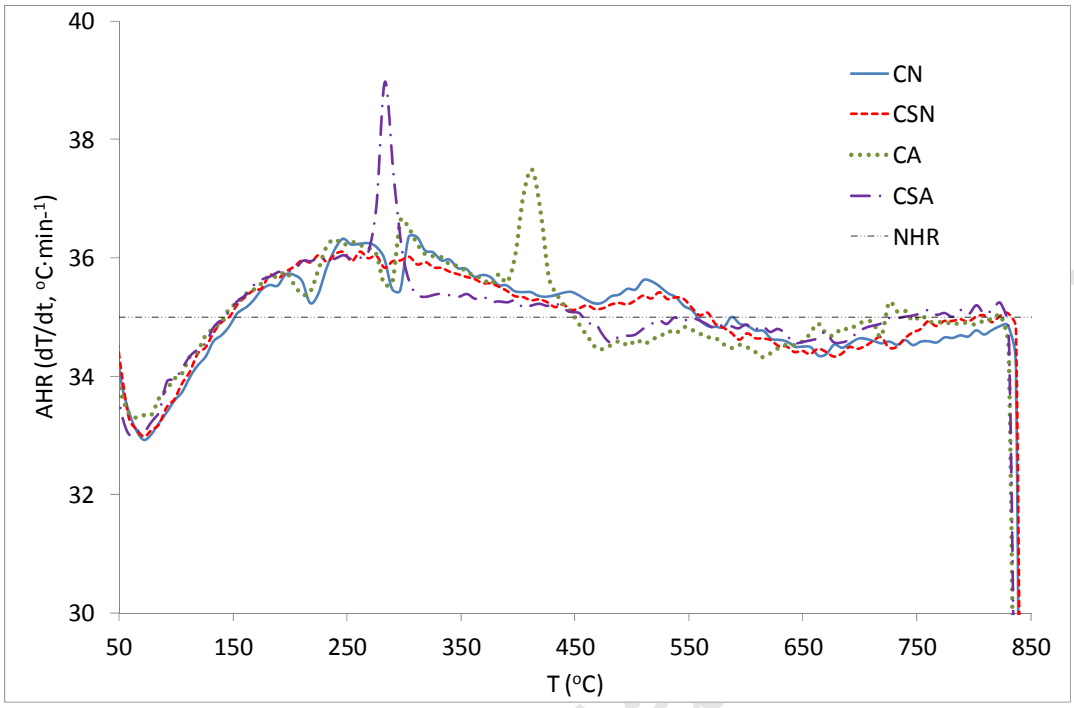

Figure 4.

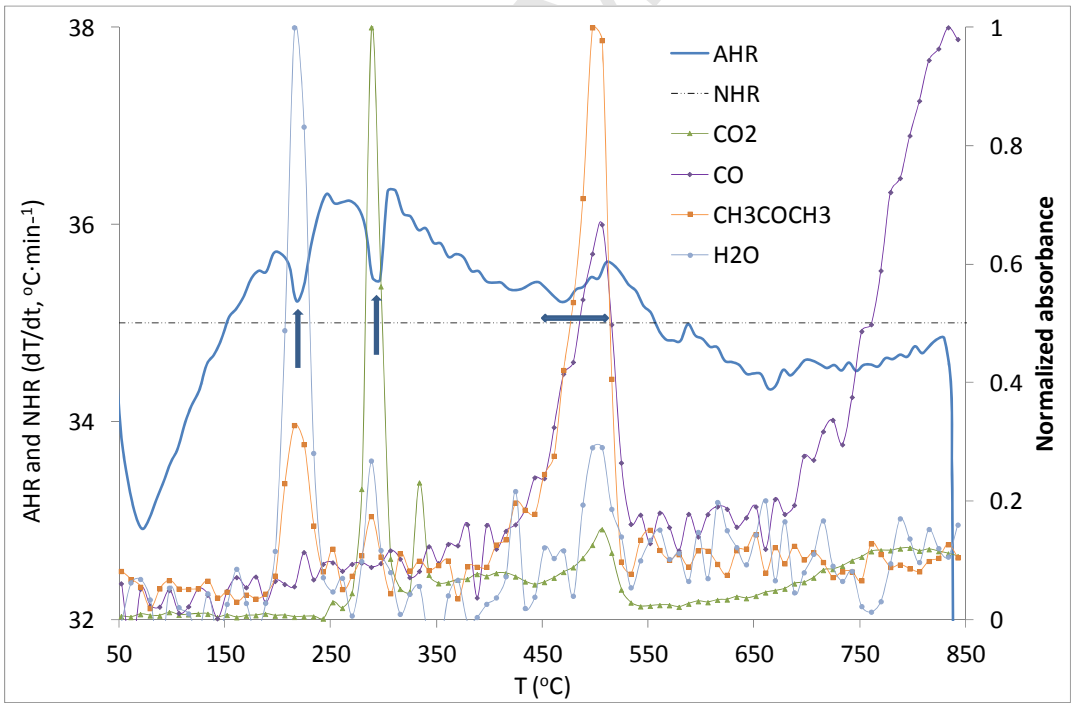

Figure 5a.

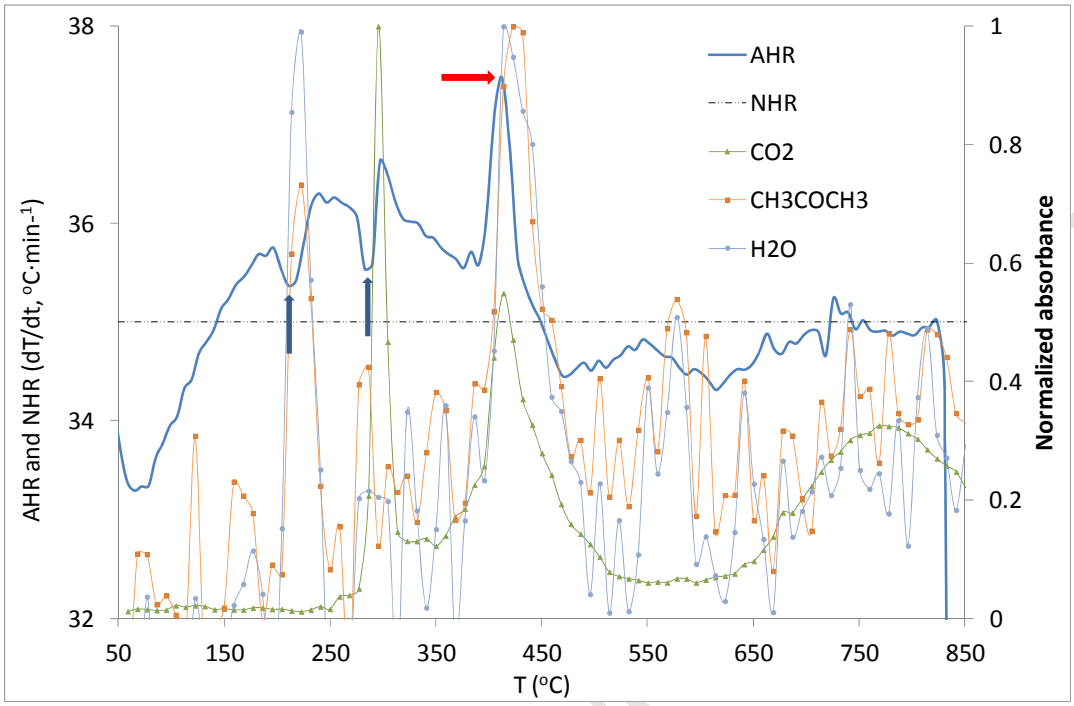

Figure 5b.

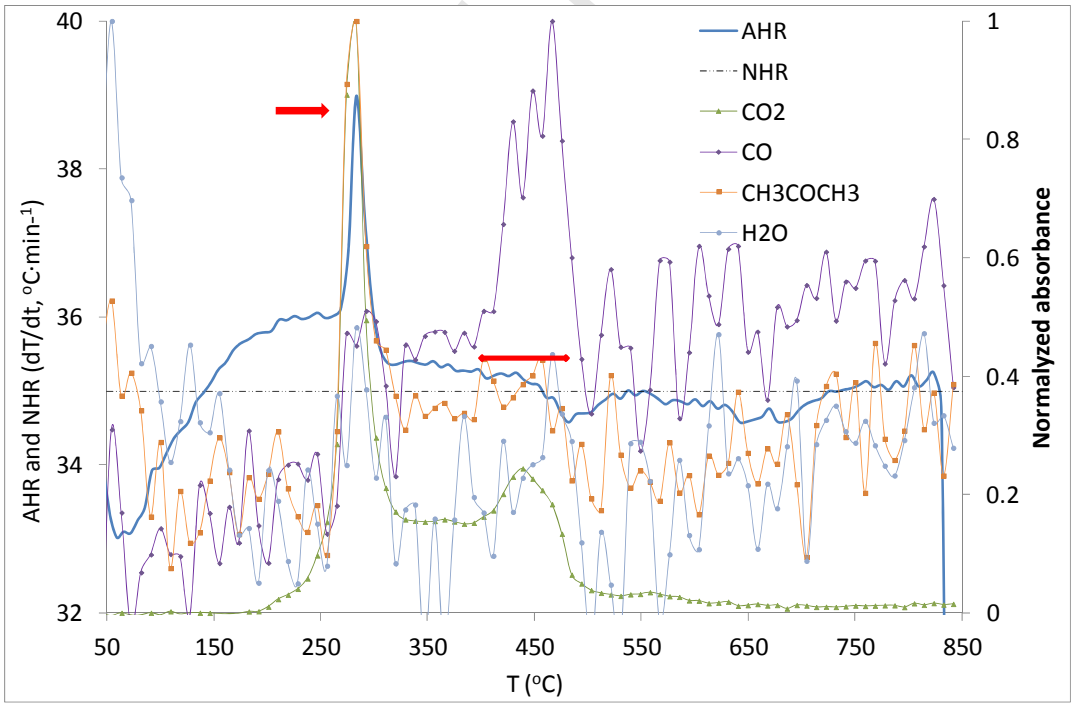

Figure 5c.

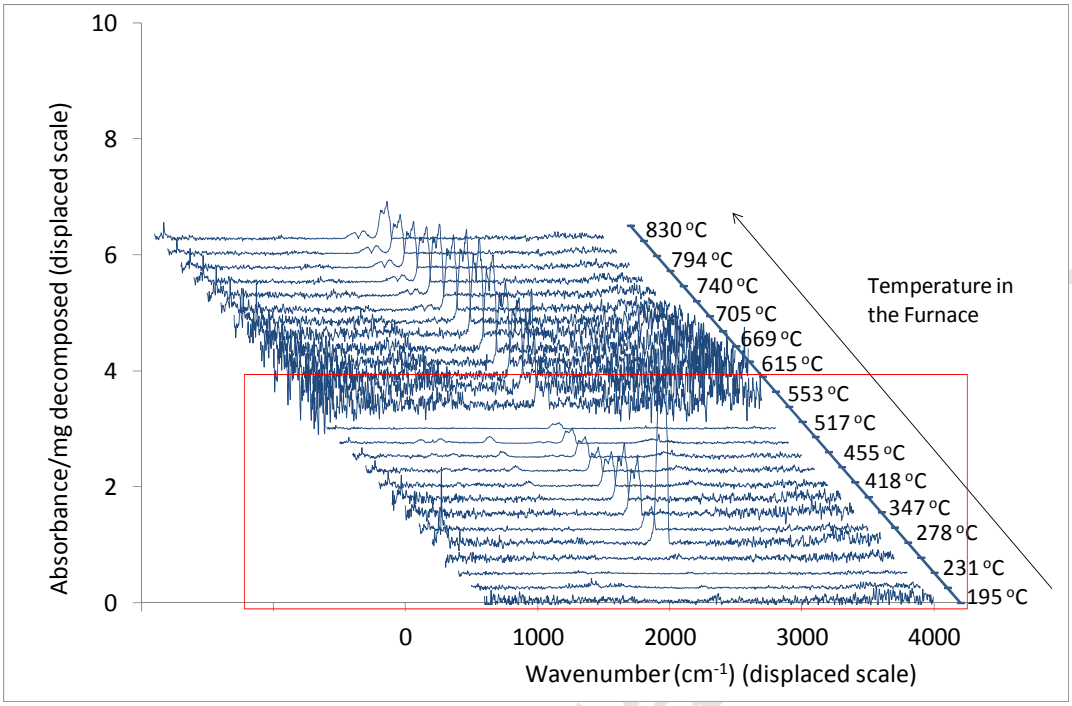

Figure 6a.

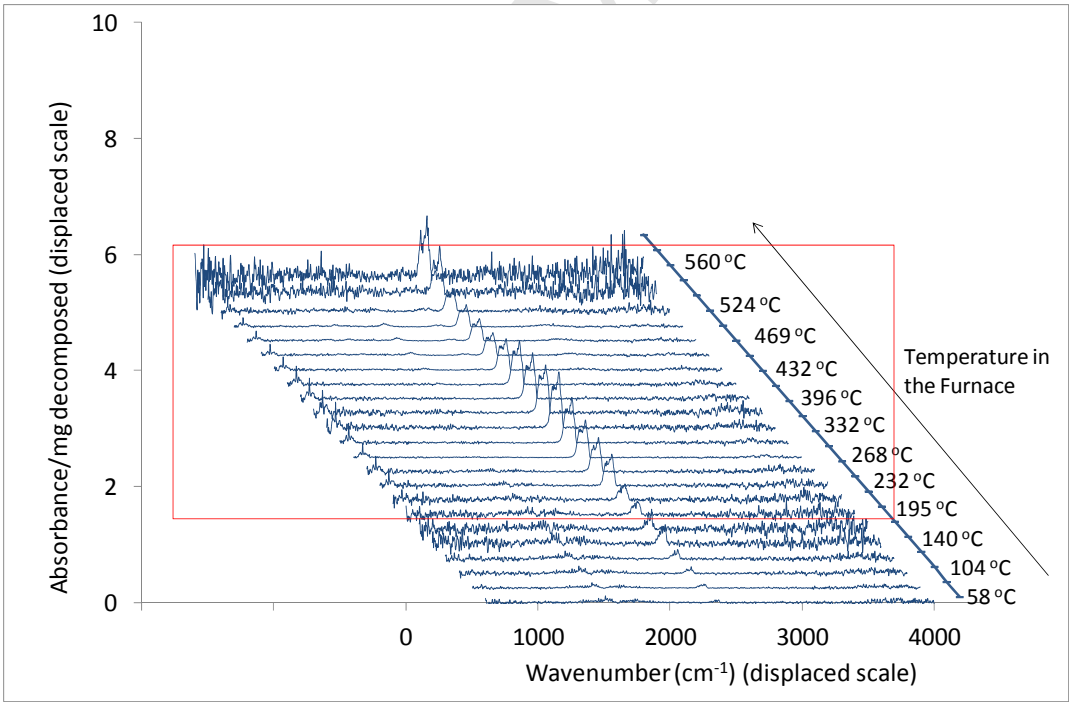

Figure 6b.

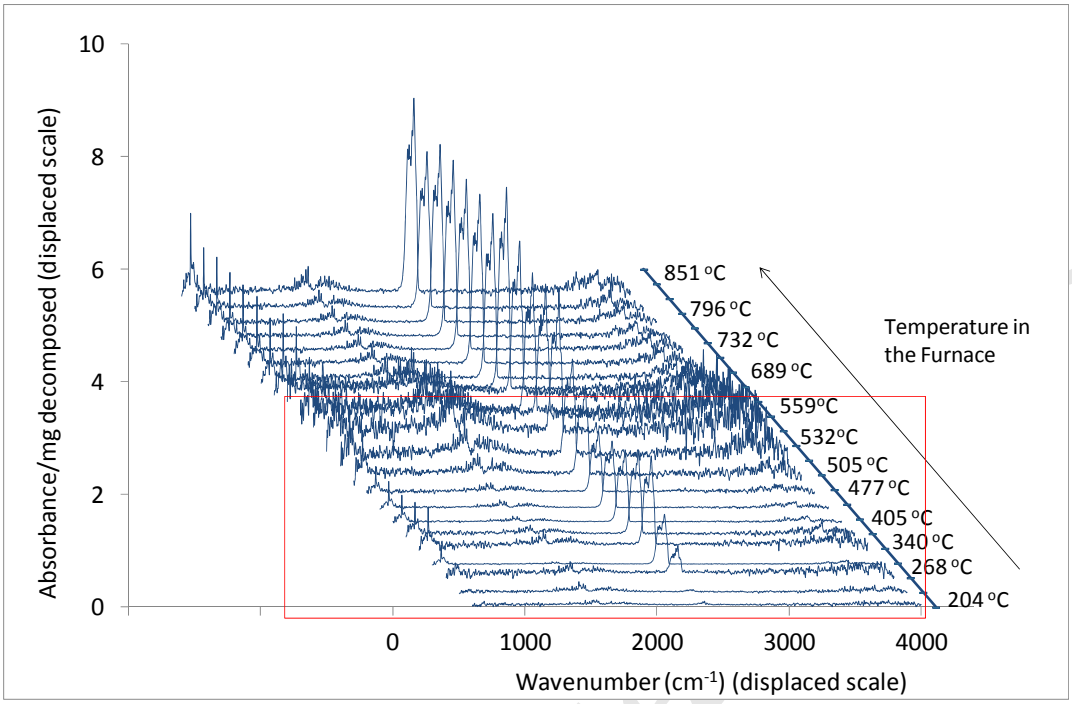

Figure 6c.

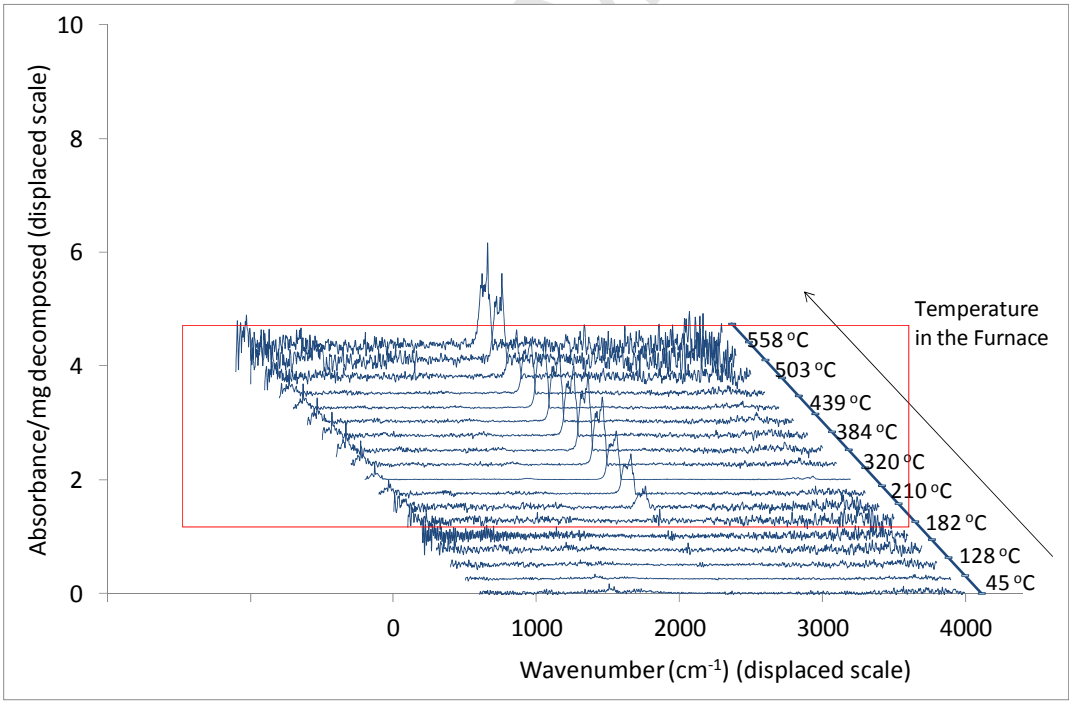

Figure 6d.

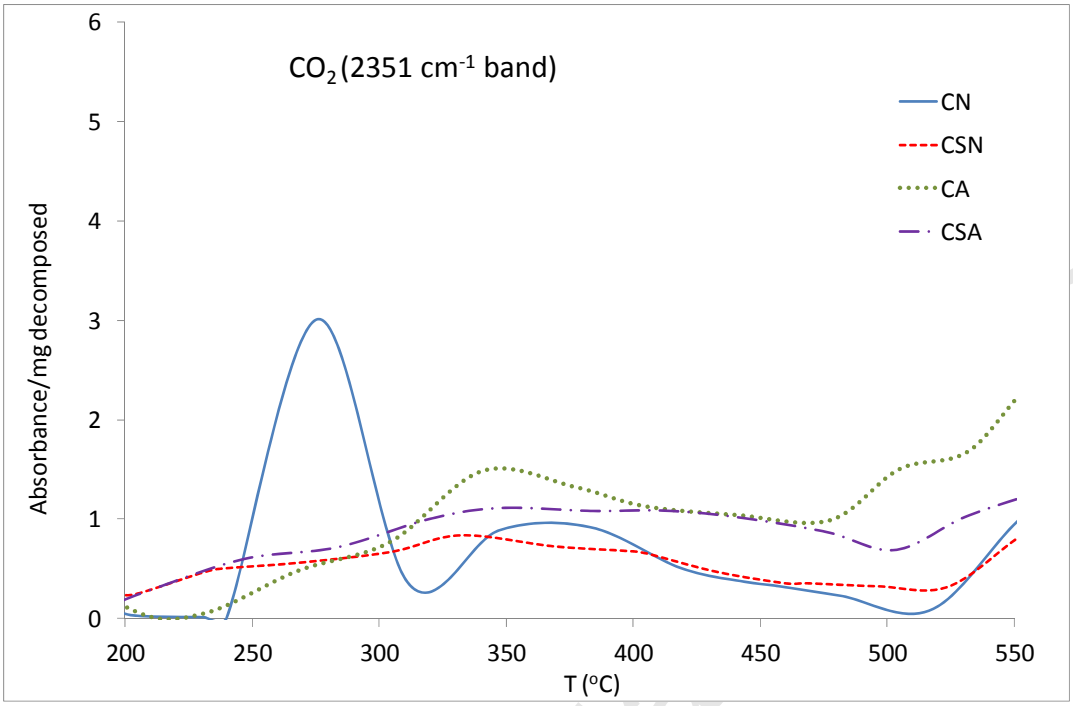

Figure 7a.

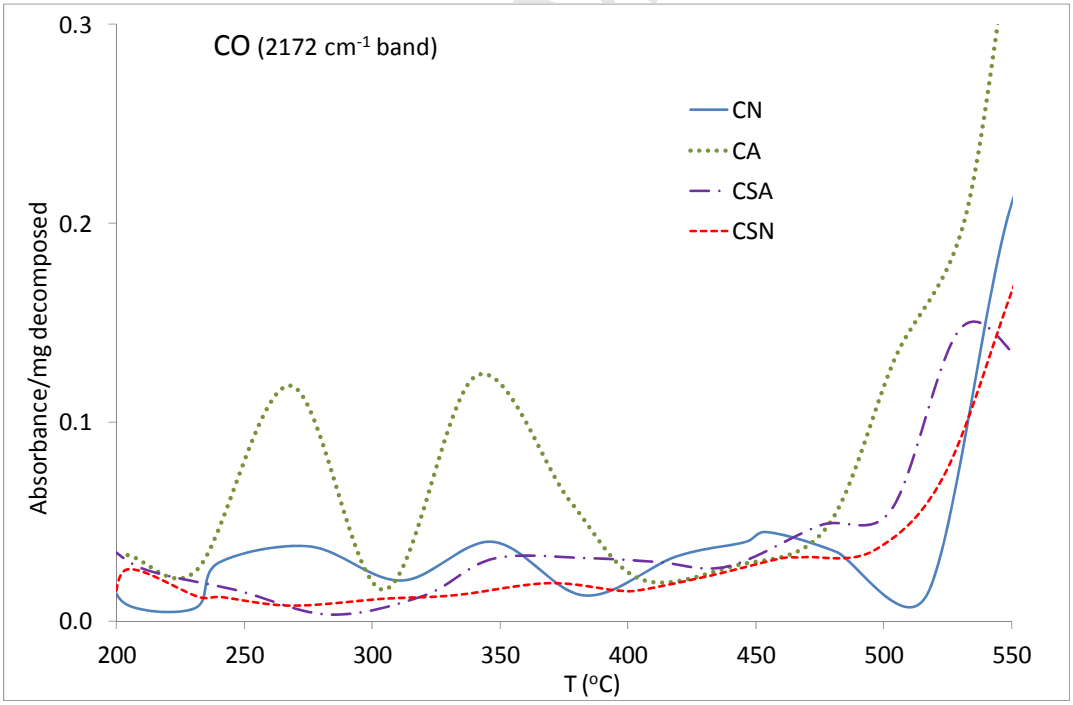

Figure 7b.

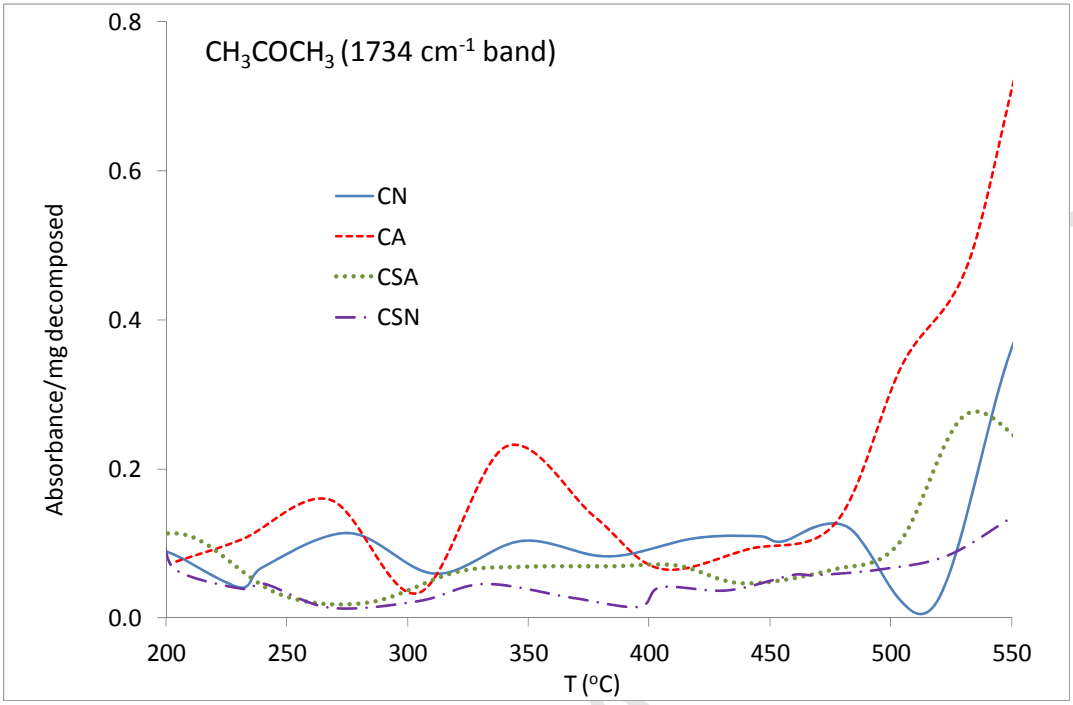

Figure 7c.